

Electrochemical Response of Glassy Carbon Electrodes Modified using Graphene Sheets of Different Sizes

K. L. S. Castro^{1,2}, S. M. Oliveira^{1,2}, R. V. Curti¹, J. R. Araújo¹, L. M. Sassi¹, C. M. Almeida¹, E. H. M. Ferreira¹, B. S. Archanjo¹, M. F. Cabral³, A. Kuznetsov¹, L. A. Sena¹, C. A. Achete¹ and E. D'Elia^{2,*}

¹ Instituto Nacional de Metrologia, Qualidade e Tecnologia, Avenida Nossa Senhora das Graças, 50, 25250-020, Duque de Caxias, RJ, Brasil.

² Instituto de Química, Universidade Federal do Rio de Janeiro, Avenida Athos da Silveira Ramos, 149, 21941-909, Ilha do Fundão, RJ, Brasil.

³ Grupo de Materiais e Superfícies Nanoestruturadas - Instituto Federal de Educação, Ciência e Tecnologia do Rio de Janeiro, Rua Senador Furtado, 121, 20270-021, Rio de Janeiro, RJ, Brasil.

*E-mail: eliane@iq.ufrj.br

Received: 6 September 2017 / Accepted: 20 October 2017 / Online Published: 1 December 2017

In this study, we investigated the electrochemical behavior of reduced graphene oxide sheets (rGO) of different sizes deposited on glassy carbon electrodes. Graphene oxide sheets were produced by the exfoliation of graphite oxide in an aqueous solution by ultrasonication. Scanning electron microscopy and transmission-mode scanning electron microscopy results indicated a decrease in the size of the graphene oxide sheets with an increase in the exfoliation time or sonication power. The results of spectroscopic characterization corroborated with this behavior. X-ray diffraction analysis indicated a broadening of the peaks with crystallite size reduction while Raman spectroscopy results suggested an increase in the structural defects in the sp^2 framework of graphene oxide. Complementary X-ray photoemission spectroscopy analysis indicated a decrease in the sp^2/sp^3 ratio with respect to the amount of sp^2 framework in graphene oxide sheets upon decreasing the sheet size. Electrochemical analysis showed that the response of the GO-modified glassy carbon electrodes increased significantly with a decrease in the graphene oxide sheet size.

Keywords: graphene oxide; graphite oxide; Hummers' method; exfoliation time; electrochemical sensors

1. INTRODUCTION

Graphene and its chemical derivatives have attracted great interest in recent years; their high mechanical strength, combined with high thermal and electrical conductivities, permits their use in various technological fields [1-3]. In particular, the electrochemical properties of graphene open up new fields of application as a construction material for high performance electrodes in ultracapacitors,

fuel cells, sensors, and batteries [4]. The method of graphene production is particularly important in determining its applicability; the chosen method should be capable of yielding a large amount of material. In this context, chemical routes are considered the most promising for large-scale production of graphene. Several chemical methods of graphene production using graphite (the most abundant and natural precursor) and other sources of carbon, such as hydrocarbons and carbides, were studied [5-9]. Generally, chemical methods consist of the initial production of graphite oxide followed by its exfoliation and reduction to obtain graphene [7, 10, 11].

The chemical route to graphene oxide synthesis can be subdivided into three main steps: oxidation of precursor, intercalation, and exfoliation [7, 10-14]. The oxidation and intercalation steps enable the onset of interactions between molecules and/or ions and graphene layers of the chosen precursor [15-17]. In this stage, functional groups such as hydroxyl, carboxyl, and epoxides are introduced into the graphite structure in between the graphene layers [2,15,18]. As a result, the raw material undergoes chemical and structural modifications defined by the formation of bonds between carbon and oxygen groups, the latter being responsible for the term graphene oxide [19]. The intercalated graphite oxide is later purified and subjected to exfoliation, which results in a mutual separation of the graphene layers and the subsequent formation of graphene oxide (GO) [11,12,20]. Normally, the exfoliation process is carried out by placing a graphite oxide solution of known concentration in the ultrasound chamber [14, 19, 21-23]. Although alternative techniques to promote GO formation have been proposed [16, 24], the ultrasound method is considered the most popular [20, 23, 25].

The subsequent reduction of GO can be carried out via chemical, thermal, or electrochemical routes [26]. Due to the inherent electrochemistry of GO [27], the electrochemical method exhibits the advantages of being fast, efficient, and less prone to contamination [28].

It is well established that one of the predominant factors affecting the electrochemical activity of sp^2 -hybridized carbon materials, such as graphite and carbon nanotubes [29, 30], is structural imperfections, i.e. bulk crystal lattice defects and edge termination of crystalline domains. However, to the best of our knowledge, there is only one study that addresses the question of heterogeneous electron transfer kinetics in electrochemical reactions in graphene [4]. Analogous to other carbon materials, the increased kinetics of electrolysis in a single foil of graphene was attributed to defect sites at the edges and boundaries of the crystalline domains [4]. Moreover, systematically higher values of standard rate constants of electron transfer during the reduction of $[Fe(CN)_6]^{3-}$ were obtained with smaller-sized graphene flakes.

The influence of degree of oxidation on the electrochemical properties of GO was investigated by cyclic voltammetry using GO as a modifier for glassy carbon electrodes (GCEs) [31]. It was shown that the electrochemical properties of GO were highly influenced by the degree of oxidation. The Peak current (I_p) values decreased with increasing levels of oxidation, thereby demonstrating a transition from metallic to semiconducting and insulating behavior. In this investigation, it is shown that this effect is more pronounced in sp^3 domains, which increased in number with increasing degree of oxidation and the disruption of graphitic stacking order.

This study analyzes the influence of graphene oxide exfoliation on the sheet size and its effect on the electrochemical response of potassium ferricyanide used as a redox probe by cyclic

voltammetry. Ultrasonication treatment, using different times and powers, was performed to prepare the graphene oxide fragments. Structural, spectroscopic, and morphological analyses of the produced GO samples were carried out to determine the main differences in their properties and to correlate with their electrochemical responses.

2. EXPERIMENTAL

2.1. Materials

All the employed materials, graphite flakes, sodium nitrate (HNO_3), potassium permanganate (KMnO_4), sulfuric acid (H_2SO_4), hydrochloric acid (HCl), hydrogen peroxide (H_2O_2), monosodium phosphate (NaH_2PO_4), disodium phosphate (Na_2HPO_4), potassium chloride (KCl), and potassium ferricyanide(III) ($\text{K}_3[\text{Fe}(\text{CN})_6]$), were purchased from Sigma-Aldrich (Saint Louis, Missouri, USA). Expanded graphite was purchased from Nacional de Grafite Ltd. (Bela Vista, São Paulo, Brazil).

All the solutions were prepared using deionized water produced by a Milli Q water purification system (Millipore, Darmstadt, Germany) with a resistivity of ca. $18 \text{ M}\Omega \text{ cm}^{-1}$. A 0.1 M phosphate buffer solution (PBS, pH 7.0) was employed as the supporting electrolyte. A $\text{K}_3[\text{Fe}(\text{CN})_6]$ solution was freshly prepared using 0.1 M KCl.

2.2. Apparatus

Scanning electron microscopy (SEM) and transmission-mode scanning electron microscopy (tSEM) images were acquired on a high-resolution SEM (Magellan 400). The SEM micrographs of the samples dropped onto a Si wafer were obtained in the secondary electron detection mode at 5 kV and 0.2 nA. Bright field tSEM images of the samples placed on a carbon-coated copper grid were obtained at 20 kV and 100 pA.

X-ray diffraction (XRD) analysis was performed on a D8 Focus diffractometer (Bruker-AXS, Karlsruhe, Germany) with Ni-filtered Cu $\text{K}\alpha$ characteristic radiation with a 2θ step of 0.02° and a collection time of 20 s per step. A thin film of GO was prepared by dripping the sample suspension onto a Si wafer and subsequently drying it in air.

Raman spectroscopy was carried out on a Renishaw inVia spectrometer with a 514.5 nm laser line at 0.1 mW with a 100X objective lens. All the spectra were obtained by the accumulation and averaging of 10 scans with an accumulation time of 10 s/scan in the region between 100 cm^{-1} and 3600 cm^{-1} . In order to account for the eventual inhomogeneity in the Raman signal across the measured sample, the averages of twenty-five measurements made at different points on the samples are reported.

X-ray photoelectron spectrometry (XPS) was performed in an ultra-high vacuum spectrometer (Omicron Nanotechnology) using Mg (1253.6 eV) as the X-ray source with the power defined by electron emission in an X-ray tube of 16 mA at a voltage of 12.5 kV. The survey spectra were obtained at an analyzer pass energy of 100 eV and a step of 0.8 eV. XPS C1s spectra were charge-corrected by shifting all the peaks to the adventitious carbon C1s binding energy of 284.8 eV, as reported elsewhere

[23–25]. The peak fitting procedure was performed using Casa XPS software. Before peak fitting, the background was subtracted using the Shirley method to account for the inelastic photoelectrons [26]. An asymmetric line shape [27] was used for the sp^2 carbon peak and a symmetric convolution of the Lorentzian lifetime and Gaussian instrumental-broadened (Voigt) line shape function was used in other components.

All electrochemical measurements were carried out using an Autolab PGSTAT 204 (EcoChimie, Utrecht, Netherlands) instrument connected to a PC running NOVA 1.11 data acquisition and treatment software. The working electrodes were modified and unmodified glassy carbon electrodes, which are described in detail in Section 2.3. The counter and reference electrodes were platinum wire and Ag/AgCl in saturated KCl, respectively.

Atomic force microscopy (AFM) analysis was carried out on a Witec Alfa 300 RA correlative Raman-AFM microscope in the tapping mode with a cantilever of 3 N/m load.

2.3. Graphene Oxide Sample Preparation

For high yield and high performance of the GO synthesized using a chemical route, a large surface area of the precursor is required [25, 26]. Expanded graphite (used in this work as a precursor) exhibits a larger surface area than other precursors, such as graphite flakes, due to the pretreatment step. Pretreatment includes the intercalation of graphene sheets by small molecules followed by subsequent heating, which eliminates the intercalating molecules [26, 28, 29]. As a result, the recovered graphite exhibits considerably smaller crystallites, which leads to a significant increase in the surface area [28]. A precursor with a large surface area interacts easily with oxidant mixtures, which in turn, promotes high yields. GO was prepared according to the Hummer's method [7]. Briefly, concentrated H_2SO_4 was added to a mixture of graphite (0.4 g) and $NaNO_3$ (0.2 g) in an ice bath. $KMnO_4$ (1.2 g) was slowly added to maintain the reaction temperature below 20 °C. The produced mixture was warmed up to 35 °C and stirred for 30 min. Subsequently, water (18.2 mL) was slowly added to the mixture; it promoted an intense exothermic reaction, which increased the temperature of the mixture to 98 °C. External heating was used to maintain the reaction temperature at 98 °C for 15 min. To stop the reaction, the reaction mixture was initially placed in an ice bath for 10 min. Later, water (55.3 mL) and 30% H_2O_2 (0.4 mL) were added to stop the reaction completely.

The product obtained was filtered and the resultant brown-colored slurry was washed with HCl solution (180 mL of water and 20 mL of 30% HCl solution) to remove any metallic ions. The slurry placed in the HCl solution was then centrifuged to remove supernatant impurities. The remaining solution was repeatedly washed with water and centrifuged to remove impurities, until the pH of the supernatant water was neutral.

Exfoliation of graphite oxide to graphene oxide was performed by the ultrasonication of graphite oxide dispersions in water (1 mg/mL). Two types of ultrasonic processors were used to prepare the GO samples with varying degrees of exfoliation and sheet sizes. The first one was an ultrasonic cleaner from Limp Sonic (Model LS-3DA-1/X, São Paulo, Brazil) with an ultrasonication power of 70 W. Using this processor, three types of GO samples were obtained by sonicating graphite

oxide for three different exhibition times: 3 h ($\text{GO}_{3\text{h}}$), 10 h ($\text{GO}_{10\text{h}}$), and 20 h ($\text{GO}_{20\text{h}}$). A second type of GO sample was obtained using an ultrasonic processor probe (Danbury, USA) from Branson (Model Sonifier 450), operating at 200 W for 30 min ($\text{GO}_{30\text{min PS}}$). Finally, water suspensions of the GO samples (1 mg/mL) were prepared. Additionally, two water suspensions, 0.5 mg/mL and 0.12 mg/mL, of the $\text{GO}_{10\text{h}}$ sample were prepared.

A sedimentation test was performed to observe the stabilization of GO dispersions in stationary conditions for twenty-four hours. In the case of graphite oxide, the dispersion was not stabilized and precipitation was observed.

2.4. Preparation of GO-Modified Electrodes and Electrochemical Measurements

The GCEs used in this study were cleaned by polishing them with alumina powder suspensions (1.0 and 0.3 μm), followed by rinsing with deionized water and sonication in diluted ethanol for 5 min to remove any alumina residues from the surfaces.

GO-modified glassy carbon electrodes (GO/GCE) were prepared by the drop-casting of 1 μL of GO suspensions onto the surfaces of cleaned GCEs, followed by drying at 50 °C in an oven. A small cavity of ca. 3 mm diameter on the top surface of the GCE electrode limited the deposition volume of the GO solution.

Electrochemical reduction of GO cast on GO/GCE was carried out by chronoamperometry with a PBS solution at -1.5 V for 60 s, resulting in the formation of reduced graphene oxide (rGO) on glassy carbon electrodes (rGO/GCE). A visual inspection of the rGO/GCE electrodes confirmed that the area of the reduced graphene is constrained to the cavity surface of the GCE electrode.

The electrochemical performance of the produced rGO/GCE electrodes was studied by cyclic voltammetry (CV) in the potential range of -0.2 to 0.6 V at a scan rate of 30 mV s^{-1} in the presence of 5 mM $\text{K}_3[\text{Fe}(\text{CN})_6]$ in 0.1 M KCl. Prior to electrochemical analysis, the dissolved oxygen present in the electrolyte solution was removed by bubbling nitrogen through the solution for 5 min.

3. RESULTS AND DISCUSSION

3.1 Structural and Morphological Analysis

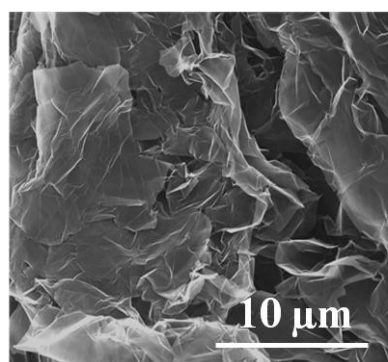


Figure 1. SEM micrograph of expanded graphite

The morphology of expanded graphite was examined by SEM (Fig. 1); a rough surface could be observed, similar to the results reported previously (Yasmin et al. [32]).

To verify the structure of expanded graphite, XRD (Fig. 2a) and Raman (Fig. 2b) analyses were carried out. The XRD patterns (Fig. 2a) of the precursor samples indicate a characteristic (002) Bragg reflection of graphite at 26.5° [33]. Figure 2b shows the Raman spectrum of expanded graphite. The band at 1580 cm^{-1} , known as the G-band, represents the in-plane stretching of carbon atoms in graphitic structures [34-37]. The presence of disorder or defects in the lattice, such as vacancies, oxygen-containing functional groups, and the adsorption of molecules on the graphitic structure surface, are revealed by the presence of another band called the D-band, which is positioned near 1350 cm^{-1} [38, 39]. The absence of this band confirms that the precursor structure is almost free of such defects.

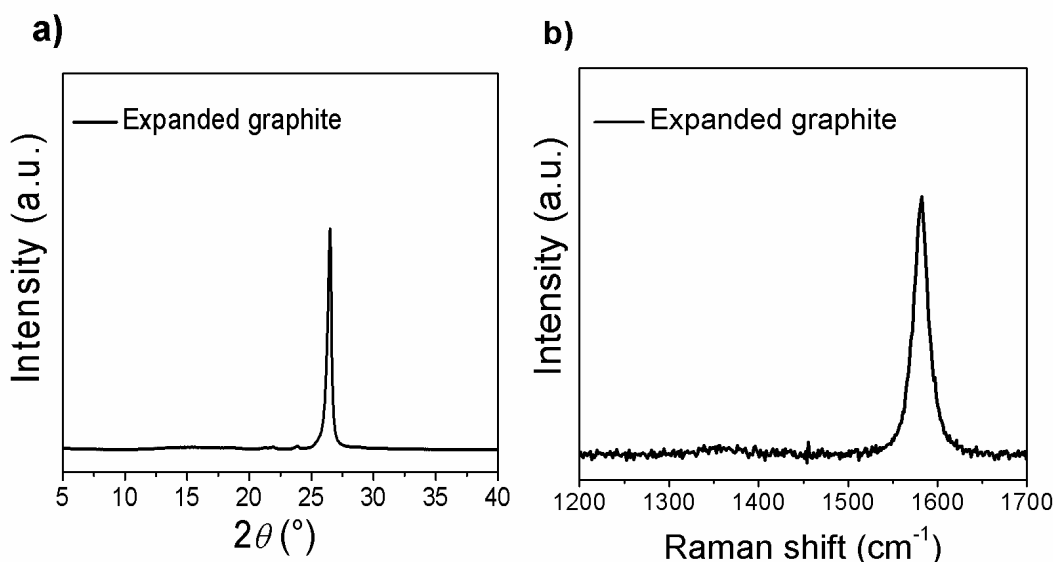


Figure 2. (a) XRD pattern and (b) Raman spectrum of expanded graphite

Figure 3 depicts the morphology (Fig. 3a), diffraction pattern (Fig. 3b), and results of the sedimentation test of graphite oxide (Fig. 3c). The tSEM image in Fig. 3a shows that the morphology of graphite oxide is analogous to that of a thin membrane. The diffraction peak observed at around 11° is characteristic of graphite oxide and graphene oxide obtained using the Hummers' method and represents an increase in the stacking periodicity due to the intercalation of oxygen atoms between the graphene layers, in comparison to graphite [20, 40, 41].

The sedimentation test results confirmed the bulk structure of graphite oxide as shown in Figures 3c and 3d. The initially homogeneous solution decanted after 24 h, whereas the graphene oxide solution was found to be stable for at least a few weeks [42].

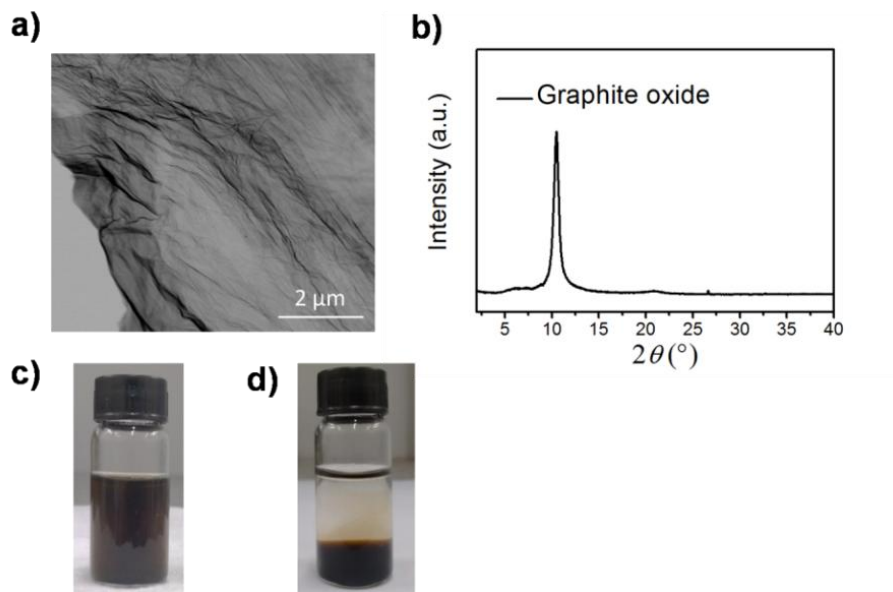


Figure 3. (a) TSEM image and (b) XRD pattern of graphite oxide. Graphite oxide solution after (c) preparation and (d) after 24 h

It is extremely important to understand the influence of ultrasonication parameters on the structural, morphological, and electrochemical properties of the produced graphene oxide sheets, as they influence the usability of the material in different technological applications [37].

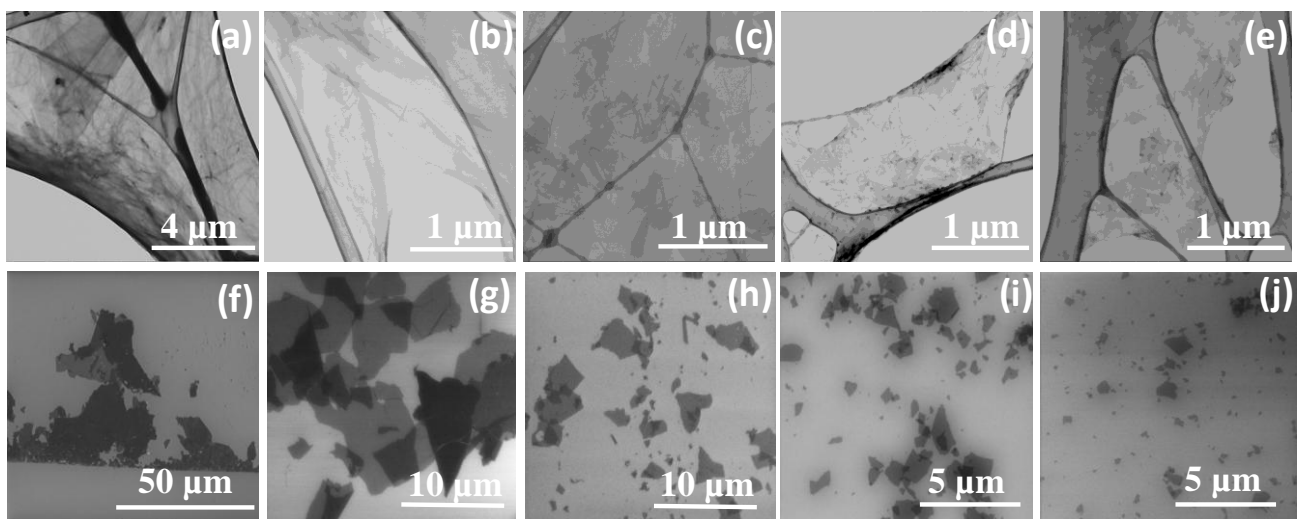


Figure 4. TSEM (Figure 4 a-e) and SEM (Figure 4 f-j) images of graphite oxide. (a, f): graphite oxide after 3 h of exfoliation, (b, g): 10 h of exfoliation, (c, h): 20 h of exfoliation, and (d, i) 30 min in a probe sonicator (e, j)

Figure 4 shows the tSEM and SEM micrographs of graphite oxide deposited on ultrathin carbon films on lacey carbon support films. The tSEM images of all the synthesized samples (Fig. 4a–e) confirm the membrane-like architecture of GO; these observations corroborate with previous reports on GO morphologies [20, 43]. Residual graphite oxide crystallites and a few layered-graphene oxide

particles dominate the tSEM and SEM micrographs of the graphite oxide sample (Fig. 4a and 4f, respectively). Ultrasonic treatment in a conventional sonicator for 3 h resulted in nearly 100% exfoliation of graphite oxide into individual GO sheets (Fig. 4b and 4g). Increasing the ultrasonication treatment time to 10 h induced fragmentation in the GO sheets; such fragmentation increased with an increase in the ultrasonication time (compare Fig. 4b, g with Fig. 4c, h and Fig. 4d, i). The probe sonicator also induced strong fragmentation in the GO sheets (Fig. 4e, j). Qualitatively, the average characteristic size (R) of the GO sheets subjected to ultrasonication was in the following order: $R_{3h} > R_{10h} > R_{20h} > R_{PS30min}$.

AFM results (Fig. 5) of the graphite oxide and graphene oxide samples obtained at different exfoliation conditions agree well with the SEM and tSEM observations on GO morphology; the AFM results also indicate an increase in GO sheet fragmentation with increasing time and/or power of ultrasound treatment. A few layers of wrinkled graphite oxide particles (Fig. 5a) appear as small GO sheets after 3 h of sonication in a conventional ultrasound bath (Fig. 5b). Further ultrasound treatment leads to a reduction in the GO sheet size (Fig. 5c and 5d). The highest extent of fragmentation could be observed in the GO samples obtained after 30 min of treatment in the probe sonicator (Fig. 5e).

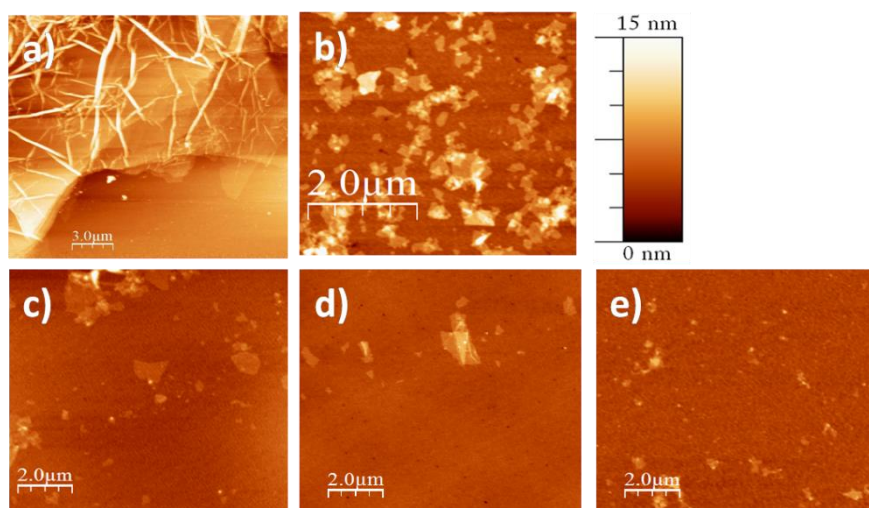


Figure 5. AFM images of (a) graphite oxide and graphene oxide after (b) 3 h, (c) 10 h, and (d) 20 h of exfoliation in a conventional ultrasound bath. (e) AFM image of graphene oxide after 30 min of exfoliation in a probe sonicator

The XRD results of the produced GO samples are shown in Fig. 6. Analogous to graphite oxide, the GO samples exhibit a characteristic XRD peak at $2\theta \approx 11^\circ$, representing a periodic stacking of the GO sheets [20, 44]. Small misfits in the peak positions of the respective samples reflect small deviations in the spacing between GO sheets. Because the peak position of graphite oxide is nearly the same (11°), one can conclude that a chemical binding of GO sheets occurs during XRD sample preparation, resulting in a formation of small crystallites of graphite oxide. Nevertheless, a clear correlation between GO sheet size and XRD peak broadening can be established. The smaller the

average size of the initial GO sheet, the larger is the broadening in the XRD peak. This result reflects that smaller GO sheets produce more disordered stacking sequences.

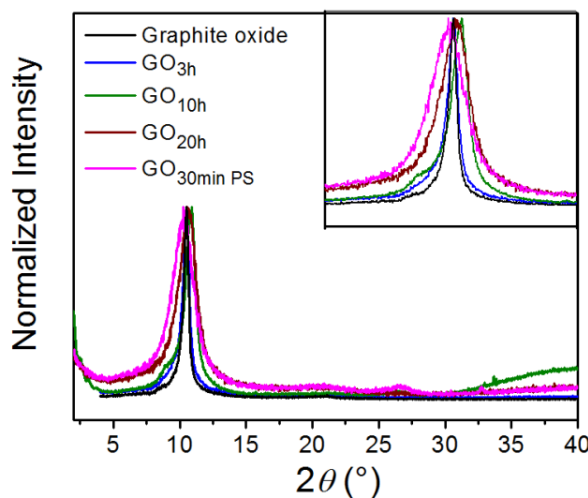


Figure 6. XRD patterns of graphite oxide (black line), graphene oxide after 3 h of exfoliation (blue line), 10 h of exfoliation (green line), and 20 h of exfoliation (brown line) in a conventional processor, and 30 min of exfoliation in a probe ultrasound processor (magenta line)

The typical Raman spectra of graphite oxide and GO samples are presented in Fig 7. As mentioned earlier, the broad G-band at 1580 cm^{-1} is a result of the in-plane vibrations of sp^2 bonded carbon atoms, producing an E_{2g} symmetry normal mode [25, 44]. The D-band centered at 1350 cm^{-1} corresponds to the A_{1g} symmetry mode produced by the out-of-plane vibrations of carbon atoms and it becomes active in the presence of structural defects [44].

Although the spectra seem to be very similar, principal component analysis (PCA) (Fig 8a) applied to the full Raman spectra distinguishes two groups of samples. The first group consists of the measurements with graphite oxide and GO samples sonicated in a conventional bath for 3 h. The second group contains the rest of the GO samples. An analysis of the ratio of the intensities of the D and G bands, I_D/I_G , as a function of the G-band width also separates the Raman measurements into the same two groups. Figure 8b shows these two groups of data points together with two theoretical calculations of the I_D/I_G ratio as a function of the G-band width [39] for a graphene sample with point-like defects and a DLC sample with border-like defects caused by the boundaries of nanocrystalline domains. The dashed line in Figure 8b represents the evolution of I_D/I_G from smaller to larger G-band width values which, in turn, are defined by decreasing distances between the point defects (or increasing point defect density) in a perfect hexagonal carbon lattice. The solid line represents I_D/I_G evolution as a function of G-band width, induced by the growing presence of linear defects. Such defects characterize the extent of borders of graphene domains free of point defects or, equivalently, the reduction in the average domain size [39]. The obtained I_D/I_G ratios and respective G-band widths for all the samples put the data points close to the solid line in Figure 8b. One can conclude that nearly point defect-free graphitic domains of very small sizes comprise the structure of the produced GO samples. According to the numerical values reported by Cançado *et al.* [39], the average size of

graphitic domains in GO sheets reduces from about 6 nm (for graphite oxide and $\text{GO}_{3\text{h}}$ sample) to below 4 nm for other GO samples.

Such a result is consistent with the general picture of the local structure of graphene oxide produced by the Hummer's method [45]; nanometer-sized domains of full 6-membered carbon rings are embedded in mostly oxidized and disordered basal planes. The obtained Raman data suggests that the fragmentation of GO sheets induced by prolonged or more powerful sonication also causes the oxidation and/or fragmentation of the graphitic regions in GO sheets.

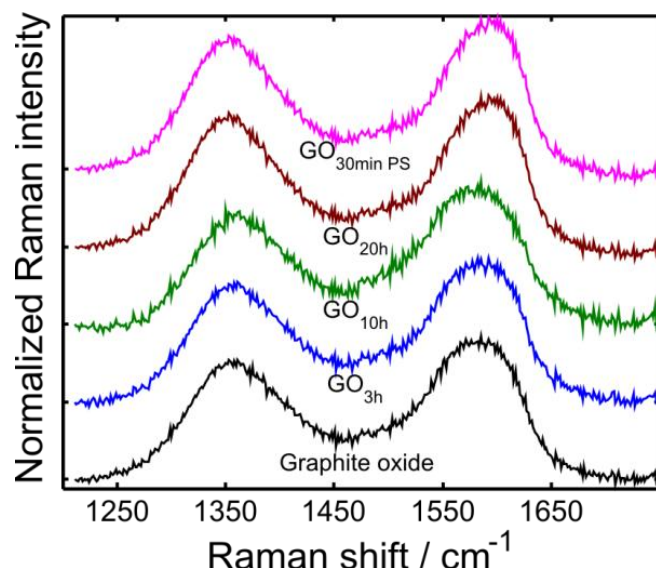


Figure 7. Raman spectra of graphite oxide (black line), graphene oxide after 3 h of exfoliation (blue line), 10 h of exfoliation (green line), and 20 h of exfoliation (brown line) in a conventional ultrasonic processor and graphene oxide after 30 min of exfoliation in a probe ultrasonic processor (magenta line)

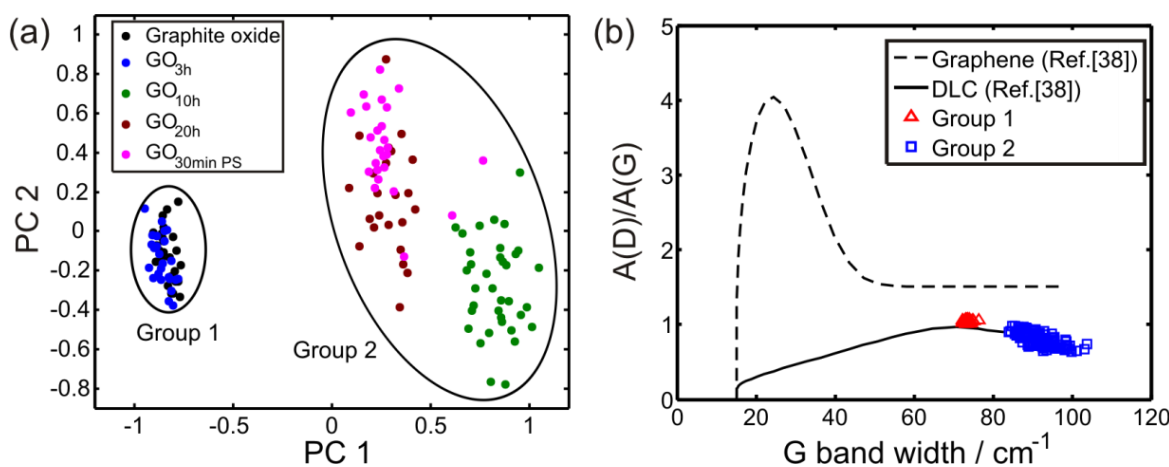


Figure 8. (a) Score plots of the principal components 1 (pc1) and 2 (pc2) from the PCA analysis of normalized Raman spectra showing two distinct groups of samples. (b) I_D/I_G ratio as a function of G-band width for the samples in group 1 and group 2 compared with theoretical curves of a graphene sample with point-like defects (dashed line) and nanocrystalline graphite (DLC) samples with different grain sizes (continuous line)

XPS analysis of the prepared samples provided valuable information on the degree of oxidation of the GO sheets. Figure 9 shows the XPS spectra of the samples in the region of C1s core electron binding energy. The C1s peaks of both aromatic (C=C peak) and oxidized carbon (C–C peak) in the carbon skeleton of graphite are reported to appear in the binding energy range of 284 eV to 285 eV [44]. Therefore, the first of the two observed C1s peaks of GO were assigned to the unoxidized sp^2 C=C graphite carbon skeleton ($284.1 \text{ eV} \pm 0.1 \text{ eV}$) and to the oxidized sp^3 C–C graphite carbon skeleton ($284.9 \text{ eV} \pm 0.1 \text{ eV}$). The second C1s peak was assumed to be composed of four higher binding energies of C1s peaks corresponding to C atoms bound to O atoms with one, two, and three valence electrons. The observed intensity distributions of the second peak were deconvoluted into peaks centered at the following energies: 286.3 eV (C-OH), 287.1 eV (C-O-C, epoxy), $288.2 \text{ eV} \pm 0.1 \text{ eV}$ (C=O, carbonyl), and $289.2 \text{ eV} \pm 0.2 \text{ eV}$ (C-OOH, carboxyl).

Table 1 shows the percentages of C1s core levels obtained by fitting the measured peaks together with the ratio between the sp^2 and sp^3 bonds.

Table 1. Component percentages based on C1s XPS peak fitting of all the samples

| Sample | C=C | C-C/C-H | C-OH | C-O-C | C=O | O=C-OH | sp^2/sp^3 |
|------------------------|------------------------|------------------------|----------|----------|------------------------|------------------------|-------------|
| | (284.1 ± 0.1) eV | (284.9 ± 0.1) eV | 286.3 eV | 287.1 eV | (288.2 ± 0.1) eV | (289.2 ± 0.2) eV | |
| Graphite oxide | 18.1 | 30.8 | 19.8 | 21.2 | 5.4 | 4.7 | 0.22 |
| GO _{3h} | 17.9 | 32.3 | 15.8 | 22.9 | 5.8 | 5.3 | 0.22 |
| GO _{10h} | 16.6 | 32.3 | 18.3 | 22.7 | 4.9 | 5.2 | 0.20 |
| GO _{20h} | 15.5 | 35.2 | 9.8 | 28.7 | 5.5 | 5.3 | 0.19 |
| GO _{30min PS} | 13.7 | 34.1 | 11.6 | 30.8 | 4.4 | 5.4 | 0.16 |

The sp^2 bonds correspond to the first component (C=C) and sp^3 bonds are formed by the C-C/C-H, C-OH, and C-O-C components. Although the last two components in Table 1 also contribute to the overall sp^2 and sp^3 bonding, the carbonyl and carboxylic acid fragments are located at the edges of the GO sheets [26] and do not contribute to sp^2 and sp^3 bonds in the basal planes.

One can see that the fragmentation of GO sheets slightly induces additional oxidation suggesting that the proportion of graphitic and oxidized regions in the produced GO sheets changes from 0.22 to about 0.16 upon fragmentation. These values are in good agreement with the results of microscopic analysis [45], which estimated the proportion of unoxidized to oxidized regions in GO sheets as 1:5 or 0.2 sp^2/sp^3 ratio.

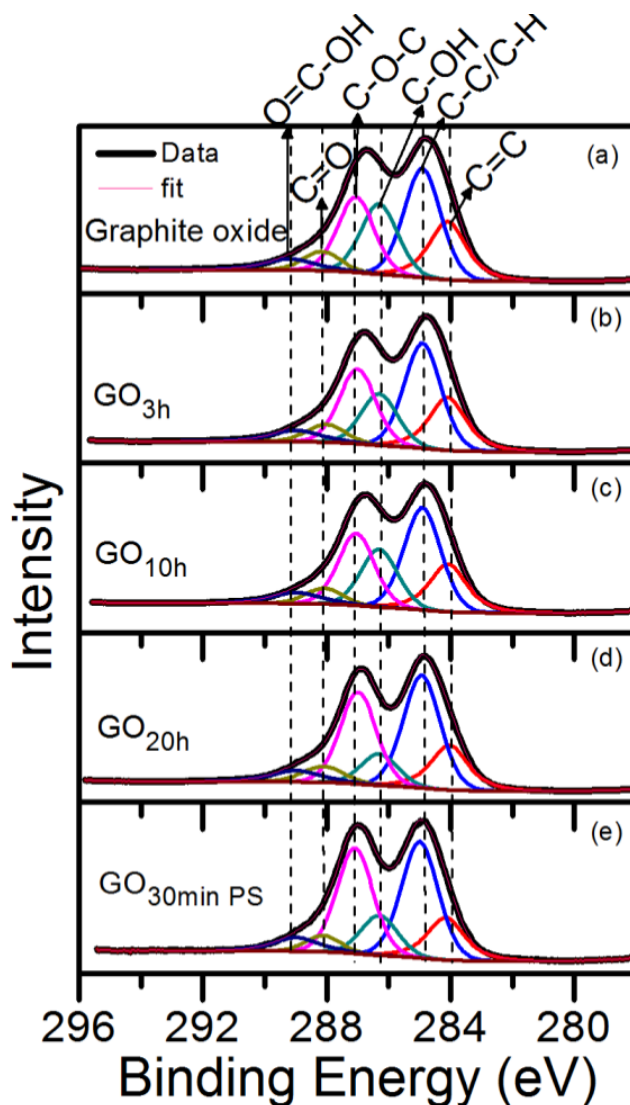


Figure 9. High resolution XPS spectra in the C1s region of (a) graphite oxide and graphene oxide after (b) 3 h of exfoliation, (c) 10 h of exfoliation, and (d) 20 h of exfoliation in a conventional ultrasonic processor and (e) 30 min of exfoliation in a probe sonicator

3.2. Electrochemical Analysis

It is generally recognized that cyclic voltammetry is not an accurate method for the quantitative characterization of electrochemical parameters, such as the concentration of electroactive species or the rate constants of electrochemical reactions [46]. However, CV is a powerful diagnostic tool that allows one to understand a system's behavior at a qualitative or semi-quantitative level and to determine other methods better suited for the precise evaluation of such parameters.

The cyclic voltammograms of all the studied electrodes modified with 1 mg/mL suspensions of the reduced graphene oxide (rGO) samples were obtained using 5 mM $K_3[Fe(CN)_6]$ in 0.1 M KCl as the supporting electrolyte (Figure 10).

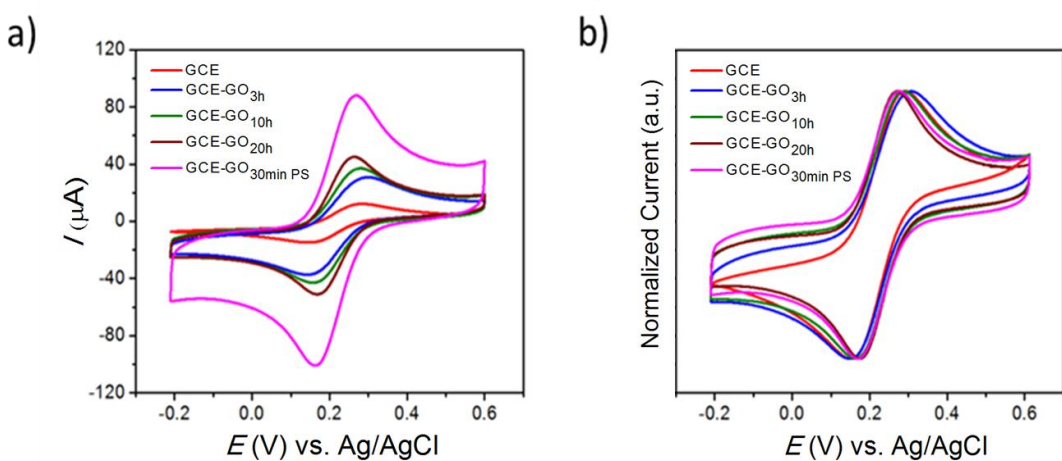


Figure 10. (a) Cyclic voltammograms of rGO-modified GCEs in 5 mM $\text{K}_3[\text{Fe}(\text{CN})_6]$ solution in 0.1 M KCl at a scan rate of 30 mV s⁻¹ and (b) normalized voltammograms. rGO deposition was performed using 1 mg/mL suspensions.

The voltammograms presented in Figure 10a indicate that graphene oxide of a small sheet size leads to an increase in the peak current. Two main factors could contribute to this observed increase – increase in the electrode area and/or electrocatalytic effect. The electrocatalytic effect does not seem to contribute much to the increase in current because the peak potential remained unchanged in all the voltammograms (Figure 10b) [49]. Therefore, the increase in current might be due to the reduction in the size of the deposited rGO fragments, which leads to an increase in the overall surface area of graphene [46-49].

Oxidation debris (OD) can be defined as highly oxidized polyaromatic fragments strongly adsorbed on the graphene matrix by $\pi-\pi$ stacking, hydrogen bonding, and van der Waals interactions [27]. Bonanni et al. studied the electrochemical behavior of graphene oxide nanoplatelets (GONPs) subjected to different extent of ultrasonication times in 0.1 M NaCl and 10 mM sodium phosphate buffer, pH 7.0 [27]. They observed voltammetric peaks around -1.4 V originated from the inherent electroactivity of GONPs and correlated to the presence and amount of oxygen functionalities on the graphene surfaces (i.e. its reduction). They showed that the intensity of the reduction peaks decreased when the ultrasonication time was extended from 2 to 24 h. This effect was attributed to the removal of oxygen functional groups present in GO after exfoliation which increases the electrochemical response of the electrode. Our results corroborate the trend in increasing the ultrasonication time and increasing the sensor electroactivity. However, in our case, a reduction process was conducted on all the GO-modified electrodes before the voltammetric study and we observed that the effect of sheet size on the peak current was dominant. Besides our work also shows the influence of the sonication power in reducing the size of the deposited rGO fragments.

Moreover, a distortion in the shapes of the anodic and cathodic waves in broader voltammograms could be observed when the size of the deposited rGO fragments was small. This behavior is due to the increase in capacitive current. Both peak current, i_p , and charging current, i_c , are proportional to the area of the electrode [46]. It is important to mention that while i_p varies with the

square root of the scan rate, i_c varies proportionally with the scan rate; therefore, i_c becomes relatively more important at faster scan rates. Consequently, in the absence of all factors influencing the Faradaic current, apart from surface area, at 30 mV s^{-1} , a relative increase in the charging current is more pronounced in the electrodes modified by highly fragmented graphene sheets. Indeed, considering the 1 mg/mL suspensions of the rGO samples used to prepare modified GCE electrodes, the relative contribution of the charging current to the total current is the highest in the case of the $\text{rGO}_{30\text{min PS}}$ sample (Figure 10b).

Although a very high overall current increase can be achieved using modified electrodes, a high charging current would limit the maximum useful amount of rGO modifier, which is a drawback for the eventual application of such modified electrodes as sensors. With the objective of studying the relative contribution of charging current to the total measured current in cyclic voltammograms, different amounts of rGO were deposited on the GCE surfaces using rGO suspensions of different concentrations. Figure 11 shows the cyclic voltammograms of the $\text{GO}_{10\text{h}}$ samples (1 mg/L , 0.5 mg/L , and 0.12 mg/L suspensions) deposited on GCE electrodes. As expected, a reduction in the peak current was observed with a decrease in the amount of deposited graphene (Figure 11a). The normalized voltammograms (Figure 11b) clearly showed a slightly broader voltammogram for the highest amount of rGO (1 mg/mL) due to the increase in the contribution of capacitive current. Moreover, it can be observed that the separation between the anodic and cathodic peaks remains the same at all rGO amounts.

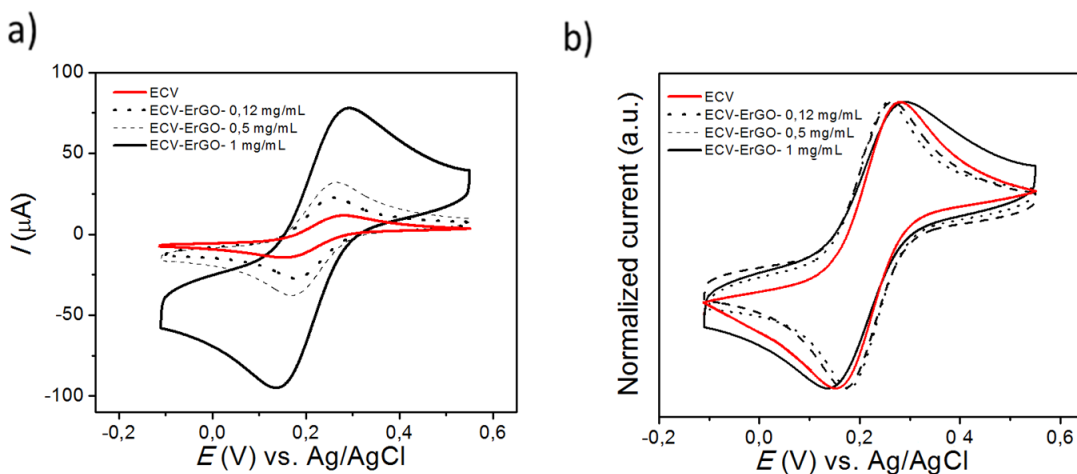


Figure 11. (a) Cyclic voltammograms of GCEs modified by $\text{GO}_{10\text{h}}$ in a $5 \text{ mM K}_3[\text{Fe}(\text{CN})_6]$ solution in 0.1 M KCl at a scan rate of 30 mV s^{-1} and (b) the corresponding normalized voltammograms. The concentrations of $\text{GO}_{10\text{h}}$ were varied between 1 mg/mL , 0.5 mg/mL , and 0.12 mg/mL .

All the described results suggest that an increase in the electrochemical response of modified electrodes can be achieved by tuning the amount and sheet size of the rGO modifier. This study could be useful for innumerable applications in analytical proposals, batteries, and fuel cells.

Though there are a number of reports on rGO-modified electrodes [50-57] as sensors for different analytical applications, there is no work relating the importance of choosing the correct GO sheet size and amount for obtaining a high electrochemical sensor response.

4. CONCLUSIONS

In conclusion, a practical and relatively simple method of glassy carbon electrode modification by graphene is described. Using cyclic voltammetry to analyze the ferricyanide/ferrocyanide redox couple electrochemical response, we show that an increase in the electrode current can be achieved by decreasing the size of the precursor graphene oxides sheets. An increase in the active surface area of the electrode along with GO exfoliation produced a greater number of edges. This behavior is pointed out as the dominating factor contributing to the overall current increase. The optimization of rGO sheet size and deposition amount may lead to an enhancement in the performance of GCEs for various electron transfer processes.

ACKNOWLEDGMENTS

The authors would like to thank CNPq, FINEP and FAPERJ for financial support.

References

1. W. Choi, I. Lahiri, R. Seelaboyina and Y. S. Kang, *Cr. Rev. Sol. State*, 35 (2010) 52.
2. F. Ali, N. Agarwall, P. K. Nayak, R. Das and N. Periasamy, *Curr. Sci. India*, 97 (2009) 683.
3. P. Avouris and C. Dimitrakopoulos, *Mater. today*, 15 (2012) 86.
4. B. Zhang, L. Fan, H. Zhong, Y. Liu and S. Chen, *J. Am. Chem. Soc.*, 135 (2013) 10073.
5. M. Eizenberg and J. M. Blakely, *Surf. Sci.*, 82 (1979) 228.
6. T. Aizawa, R. Souda, S. Otani, Y. Ishizawa and C. Oshima, *Phys. Rev. Lett.*, 64 (1990) 768.
7. W. S. Hummers and R. E. Offeman, *J. Am. Chem. Soc.*, 80 (1958), 1339.
8. L. Xuekun, Y. Minfeng, H. Hui and S. R. Rodney, *Nanotech.*, 10 (1999) 269.
9. K. S. Novoselov, A. K. Geim, S. V. Morozov, D. Jiang, Y. Zhang, S. V. Dubonos, I. V. Grigorieva and A. A. Firsov, *Sci.*, 306 (2004) 666.
10. S. Park and R. Ruoff, *Nat. Nanotec.*, 50 (2009) 1.
11. Y. Zongronga, L. Xuemeia, Q. Yua and L. Jieb, *Mat. Res. Bull.*, 43 (2008) 2677.
12. J. M. McAllister, J.-L. Li, H. D. Adamson, C. H. Schniepp, A. A. Abdala, J. Liu, H. M. Alonso, D. L. Milius, R. Car, K. R. Prud'homme and A. I. Aksay, *Chem. Mat.*, 19 (2007) 4396.
13. A. M. Dimiev and J. M. Tour, *ACS Nano*, 8 (2014) 3060.
14. D. P. Hansora, N. G. Shimpi and S. Mishra, *JOM*, 67 (2015) 2855.
15. H. He, J. Klinowski, M. Forster and A. Lerf, *Chem. Phys. Lett.*, 287 (1998) 53.
16. I. Ogino, Y. Yokoyama, S. Iwamura and S. R. Mukai, *Chem. Mat.*, 26 (2014) 3334.
17. A. Lerf, H. He, M. Forster and J. Klinowski, *J. Phy. Chem. B*, 102 (1998) 4477.
18. D. Li, M. B. Muller, S. Gilje, R. B. Kaner and G. G. Wallace, *Nat. Nano*, 3 (2008) 101.
19. J. I. Paredes, S. Villar-Rodil, A. Martínez-Alonso and J. M. D. Tascón, *Langmuir*, 24 (2008) 10560.

20. D. C. Marcano, D. V. Kosynkin, J. M. Berlin, A. Sinitskii, Z. Sun, A. Slesarev, L. B. Alemany, W. Lu and J. M. Tour, *ACS Nano*, 4 (2010) 4806.
21. T. Rattana, S. Chaiyakun, N. Witit-anun, N. Nuntawong, P. Chindaudom, S. Oaew, C. Kedkeaw and P. Limsuwan, *Procedia Eng.*, 32 (2012) 457.
22. G. Chen, W. Weng, D. Wu, C. Wu, J. Lu, P. Wang and X. Chen, *Carbon*, 42 (2004) 753.
23. S. Park, J. An, R. D. Piner, I. Jung, D. Yang, A. Velamakanni, S. T. Nguyen and R. S. Ruoff, *Chem. Mat.*, 20 (2008) 6592.
24. Y. Zhu, M. D. Stoller, W. Cai, A. Velamakanni, R. D. Piner, D. Chen and R. S. Ruoff, *ACS Nano*, 4 (2010) 1227.
25. S. Stankovich, D. A. Dikin, R. D. Piner, K. A. Kohlhaas, A. Kleinhammes, Y. Jia, Y. Wu, S. T. Nguyen and R. S. Ruoff, *Carbon*, 45 (2007) 1558.
26. D. R. Dreyer, S. Park, C. W. Bielawski and R. S. Ruoff, *Chem. Soc. Rev.*, 39 (2010) 228.
27. A. Bonanni, A. Ambrosi, C. K. Chua and M. Pumera, *ACS nano*, 8 (2014) 4197.
28. Y. Gong and C. Pan, *MRS Advances*, 62 (2017) 1.
29. A. Ambrosi and M. Pumera, *Chem. - Eur. J.*, 16 (2010) 10946.
30. P. R. Unwin, A. G. Güell and G. Zhang, *Acc. Chem. Res.*, 49 (2016) 2041.
31. K. Krishnamoorthy, M. Veerapandian, K. Yun and S. J. Kim, *Carbon*, 53 (2013) 38.
32. A. Yasmin, J.-J. Luo and I. M. Daniel, *Compos. Sci. Technol.*, 66 (2006) 1182.
33. M. J. McAllister, J.-L. Li, D. H. Adamson, H. C. Schniepp, A. A. Abdala, J. Liu, M. Herrera-Alonso, D. L. Milius, R. Car, R. K. Prud'homme and I. A. Aksay, *Chem. Mat.*, 19 (2007) 4396.
34. K. Krishnamoorthy, G.-S. Kim and S. J. Kim, *Ultrason. Sonochem.*, 20 (2013) 644.
35. A. Kaniyoor and S. Ramaprabhu, *AIP Adv.*, 2 (2012) 032183.
36. A. Jorio, R. Saito, G. Dresselhaus and M. S. Dresselhaus, *Raman Spectroscopy in Graphene Related Systems*, Wiley-VCH Verlag GmbH & Co., 2011.
37. J. Ribeiro-Soares, L. G. Cançado, N. P. S. Falcão, E. H. Martins Ferreira, C. A. Achete and A. Jorio, *J. Raman Spectrosc.*, 44 (2013) 283.
38. P. R. S. Ado Jorio, Dr. Gene Dresselhaus, Prof. Mildred S. Dresselhaus, *Wiley, Germany*, 2011.
39. L. G. Cançado, A. Jorio, E. H. M. Ferreira, F. Stavale, C. A. Achete, R. B. Capaz, M. V. O. Moutinho, A. Lombardo, T. S. Kulmala and A. C. Ferrari, *Nano Letters*, 11 (2011) 3190.
40. L. Sun and B. Fugetsu, *Mat. Lett.*, 109 (2013) 207.
41. L. Stobinski, B. Lesiak, A. Malolepszy, M. Mazurkiewicz, B. Mierzwa, J. Zemek, P. Jiricek and I. Bieloshapka, *J. Electron. Spectrosc. Relat. Phenom.*, 195 (2014) 145.
42. D. Konios, M. M. Stylianakis, E. Stratakis and E. Kymakis, *J. Colloid Interface Sci.*, 430 (2014) 108.
43. C. Botas, P. Álvarez, C. Blanco, R. Santamaría, M. Granda, P. Ares, F. Rodríguez-Reinoso and R. Menéndez, *Carbon*, 50 (2012), 275.
44. K. L. S. Castro, R. V. Curti, J. R. Araujo, S. M. Landi, E. H. M. Ferreira, R. S. Neves, A. Kuznetsov, L. A. Sena, B. S. Archanjo and C. A. Achete, *Thin Solid Films*, 610 (2016) 10.
45. K. Erickson, R. Erni, Z. Lee, N. Alem, W. Gannett and A. Zettl, *Adv. Mat.*, 22 (2010) 4467.
46. A. Bard and L. Faulkner, *Electrochemical Methods: Fundamentals and Applications*, John Wiley & Sons, Inc, 2001.
47. C. Tan, J. Rodríguez-López, J. J. Parks, N. L. Ritzert, D. C. Ralph and H. D. Abruña, *ACS Nano*, 6 (2012) 3070.
48. R. Sharma, J. H. Baik, C. J. Perera and M. S. Strano, *Nano Letters*, 10 (2010) 398.
49. R. L. McCreery, *Chem. Rev.*, 108 (2008) 2646.
50. N. Kumar, R. Rajendra and N. Goyal, *Sensor Actuat. B-Chem*, 243 (2017) 658.
51. A. M. H. Ng, Kenry, C. T. Lim, H. Y. Low and K. P. Loh, *Biosens. Bioelectron.*, 65 (2015) 265.
52. S. Bozkurt, B. Tosun, B. Sen, S. Akocak, A. Savk, M. F. Ebeoglugil and F. Sen, *Anal. Chim. Acta*, 989 (2017) 88.

53. F. H.Cincotto, D. L.C.Golinelli, Sergio A. S. Machado and F. C.Moraes, *Sensor Actuat. B-Chem*, 239 (2017) 448.
54. S. Palanisamy, B. Thirumalraj, S-M. Chen, Y-T. Wang, V. Velusamy and S. K. Ramaraj, *Nature*, 6 (2016) 33599.
55. L. Luo, L. Xu and H. Zhao, *Mater. Sci. Eng. C*, 78 (2017) 198.
56. Y-H. Kim, K. Lee, H. Jung. H. K. Kang, J. Jo, I-K. Park and H. H. Lee, *Biosens. Bioeletron.*, 15 (2017) 473.
57. K. K. Sadasivuni, A. Kafy, H-C. Kim, H-U. Ko, S. Mun and J. Kim, *Synth. Met.*, 206 (2015) 154.

© 2018 The Authors. Published by ESG (www.electrochemsci.org). This article is an open access article distributed under the terms and conditions of the Creative Commons Attribution license (<http://creativecommons.org/licenses/by/4.0/>).